Corresponding author: V.V. Atuchin
Institute of Semiconductor Physics, Novosibirsk 630090, Russia
Phone: +7 (383) 3308889
E-mail: atuchin@isp.nsc.ru

Structural and spectroscopic properties of new noncentrosymmetric self-activated borate $Rb_3EuB_6O_{12}$ with B_5O_{10} units

V.V . Atuchin[1,2,3,4], A.K. Subanakov[5], A.S. Aleksandrovsky[6,7], B.G. Bazarov[5], J.G. Bazarova[5], T.A. Gavrilova[8], A.S. Krylov[9], M.S. Molokeev[10,11,12], A.S. Oreshonkov[9,13], S.Yu. Stefanovich[14]

[1]Laboratory of Optical Materials and Structures, Institute of Semiconductor Physics, SB RAS, Novosibirsk 630090, Russia

[2]Functional Electronics Laboratory, Tomsk State University, Tomsk 634050, Russia

[3]Laboratory of Semiconductor and Dielectric Materials, Novosibirsk State University, Novosibirsk 630090, Russia

[4]Laboratory of Single Crystal Growth, South Ural State University, Chelyabinsk 454080, Russia

[5]Baikal Institute of Nature Management, SB RAS, Ulan-Ude 670047, Russia

[6]Laboratory of Coherent Optics, Kirensky Institute of Physics, Federal Research Center KSC SB RAS, Krasnoyarsk 660036, Russia

[7]Institute of Nanotechnology, Spectroscopy and Quantum Chemistry, Siberian Federal University, Krasnoyarsk 660041, Russia

[8]Laboratory of Nanodiagnostics and Nanolithography, Institute of Semiconductor Physics, SB RAS, Novosibirsk 630090, Russia

[9]Laboratory of Molecular Spectroscopy, Kirensky Institute of Physics, Federal Research Center KSC SB RAS, Krasnoyarsk 660036, Russia

[10]Laboratory of Crystal Physics, Kirensky Institute of Physics, Federal Research Center KSC SB RAS, Krasnoyarsk 660036, Russia

[11]Department of Physics, Far Eastern State Transport University, Khabarovsk 680021, Russia

[12]Siberian Federal University, Krasnoyarsk 660079, Russia

[13]Department of Photonics and Laser Technologies, Siberian Federal University, Krasnoyarsk 660079, Russia

[14]Department of Chemistry, Lomonosov Moscow State University, Moscow 119991, Russia

Abstract

New noncentrosymmetric double borate $Rb_3EuB_6O_{12}$ was synthesized by the solid state reaction method, and its crystallographic parameters were obtained by Rietveld analysis. This borate crystallizes in the trigonal space group *R*32 with cell parameters a = 13.4604(2) Å, c = 30.7981(5) Å, Z = 15. Its structure features a three-dimensional framework composed of the $[B_5O_{10}]^{5-}$ groups that are bridged by Eu-O polyhedra. The existence of B_5O_{10} group in the structure was confirmed by vibrational spectroscopy. $Rb_3EuB_6O_{12}$ melts incongruently at 1101 K. The second harmonic generation effect of $Rb_3EuB_6O_{12}$ is 16 times higher than that of the α-quartz standard. In the luminescence spectrum, the domination of a single prominent narrow line from the hypersensitive $^5D_0$ - $^7F_2$ manifold of Eu^{3+} ions is observed, while the $^5D_0$ - $^7F_1$ manifold and ultranarrow $^5D_0$ - $^7F_0$ line are of comparable peak intensity. These features are explained by a specific local symmetry of the Eu ion within the crystal structure of $Rb_3EuB_6O_{12}$.

Keywords: Rubidium rare earth borate; Solid state reaction; Rietveld refinement; Raman; IR, luminescence

1. Introduction

During the last decades, borate crystals were extensively studied mainly in connection with the valuable properties of several nonlinear optical (NLO) borate crystals discovered in the past. Among the most attractive features of borate crystals are such key characteristics as their transparency in a deep UV range, high optical damage threshold combined with appropriate nonlinearity, and suitable chemical stability of optical surface should be pointed: they define wide applications of borate materials in modern laser optics and nanophotonics [1-11]. Within borate matrices, boron ions can be either three- or four-fold coordinated, and the combination of BO_4 and BO_3 units produces a large variety of crystal structures with different properties [12-15]. In recent years, many complex borate crystals were discovered and evaluated in searching for new efficient polyfunctional materials for nonlinear optics and photonics [16-23].

One of the extensively studied trends concerning borate crystals is doping them with rare earth ions producing either phosphors or lasing crystals with the possibility of simultaneous frequency doubling of generated radiation within the same crystal. Such noncentrosymmetric (NCS) borates as $YAl_3(BO_3)_4$ (YAB) [24] $Ca_4RO(BO_3)_3$ (R = rare earth of Y) [25] and $Na_3La_9O_3(BO_3)_8$ [26] are known as self-frequency doubling (SFD) materials, when doped with Nd. $YAl_3(BO_3)_3$ doped with Mn^{4+} or pair Yb^{3+}/Tm^{3+}, is prospective as an efficient phosphor material [27,28]. Femtosecond pulse generation was carried out in the $Ca_3Gd_2(BO_3)_4$:Nd^{3+} crystal [29]. However, within $M_2O–RE_2O_3–B_2O_3$ (M = alkali metal, RE = rare earth) systems, only several NCS crystalline media have been found up to date: namely, $Na_3La_2(BO_3)_3$ [30], $Rb_3Y_2B_3O_9$ [31] $Na_3La_9O_3(BO_3)_8$ [32], $K_3REB_6O_{12}$ (RE = Y, Eu, Tb, Lu) [33-36] and $Rb_3NdB_6O_{12}$ [37]. It is worth noting that $K_3REB_6O_{12}$ (RE = Y, Eu, Tb, Lu) and $Rb_3NdB_6O_{12}$ are related to the same structure type, and they crystallize in trigonal space group *R*32 and exhibit a noticeable SHG signal. The UV cut-off edge of $K_3YB_6O_{12}$ and $Rb_3NdB_6O_{12}$ is reported to be at 195-197 nm [33,37]. These findings indicate that the $M_2O–RE_2O_3–B_2O_3$ ternary systems are complex enough, and other NCS borate crystals, transparent in UV range, can be formed. In the

present study, we employ larger alkali ions since they could have a stronger polarizability and, hence, a stronger overall NLO response can be expected. The structural and optical properties of $Rb_3Y_2B_3O_9$ have not being investigated up to date. Recently, we reported on the properties of the new noncentrosymmetric borate crystal, $Rb_3NdB_6O_{12}$ [37], which is featured by an unusual blue shift of luminescent lines with respect to traditional laser materials. This shift is larger than that in other borate family: namely, huntites, and it is close to that observed in fluorides. The observed peculiarity must be ascribed to a specific influence of the current boron-based framework structure. Respectively, it is interesting to examine the properties of other rare earth ions in the same structure. In the present study, the synthesis of new crystal $Rb_3EuB_6O_{12}$ is performed. Its structural and vibrational characteristics are investigated, and the luminescent properties of Eu^{3+} ion are studied in this new borate structure.

2. Experimental

The samples were prepared by solid state reactions using high-purity starting reagents (Red Chemist, Ltd., Russia): Rb_2CO_3 (99.9%), RE_2O_3 (RE = Eu) (99.99%), and H_3BO_3 (99.99%). Before weighing, Rb_2CO_3 was preheated at 900°C for 24 h to remove any absorbed water. The reagents were weighed on an analytical balance at the accuracy of 0.5 mg. The mixtures of Rb_2CO_3, RE_2O_3, and H_3BO_3 in stoichiometric proportions were thoroughly ground in an agate mortar, slowly heated in a muffle furnace to 500°C at the rate of 1°C/min and held at this temperature for 24 h. Then, the samples were reground and annealed at 700–750°C for 24–72 h until reaching equilibrium. Temperatures were measured with a Pt–PtRh thermocouple. The temperature was controlled to be within ±2°C up to 1200°C with an OMRON controller. The equilibrium was specified when two successive heat treatments resulted in the identical X-ray patterns.

The powder X-ray diffraction data were recorded by a D8 ADVANCE Bruker AXS diffractometer (Vantec-1 detector) at room temperature using the CuK_α radiation and scanning

over the range of 2θ = 8-100°. The step size of 2θ was 0.021° and the counting time was 10 s per step. The Rietveld refinement was implemented using TOPAS 4.2 [38]. Almost all peaks were indexed by a trigonal cell (space group *R*32) with the parameters close to those of $K_3YB_6O_{12}$ [33].

Differential scanning calorimetric (DSC) measurements were performed on a STA 449 F1 Jupiter thermoanalyzer (NETZSCH) over the temperature range of 30–900°C in an argon flow. Pt crucibles were used as vessels. Pt–PtRh thermocouples were used for the measurement. The temperature measurement precision was ±1°C. The heating and cooling rates were 10°C/min. The second harmonic generation (SHG) response of powder samples was measured with a Q-switched YAG:Nd laser at λ_ω=1064 nm in the reflection mode. The SHG signal intensities ($I_{2\omega}$) from the sample and from the reference sample (polycrystalline α-SiO_2) were registered comparatively. The infrared (IR) spectra were carried out to specify the boron coordination in the new compounds. The mid-infrared spectra were obtained at room temperature using a Nicolet-380 infrared spectrophotometer with KBr pellets as standards. The spectra were obtained in the range from 500 to 2000 cm^{-1} with the resolution of 1 cm^{-1}.

3. Results and discussions

The synthesized product was a free-flowing powder. Examination of the XRD pattern of the synthesized compound revealed its close similarity to that of $K_3YB_6O_{12}$. Therefore, the initial structure model and atomic positions of $K_3YB_6O_{12}$ were adopted for the structure refinement. $Rb_3EuB_6O_{12}$ crystallizes in noncentrosymmetric space group *R*32, as it was supported by SHG measurements. The intensity of the green light (λ = 532 nm) produced by $Rb_3EuB_6O_{12}$ is about 16 of that produced by the α-quartz standard. The intensity of SHG effect is similar to that of $K_3YB_6O_{12}$ [33]. The weak SHG effect of $Rb_3EuB_6O_{12}$ and $K_3YB_6O_{12}$ is due to the B_5O_{10} groups which are aligned in the almost opposite directions and, consequently, contribute little to the SHG effect.

The refinement results and atomic coordinates obtained for $Rb_3EuB_6O_{12}$ are summarized in Tables 1, 2 and the final Rietveld profiles are shown in Fig. 1. The $Rb_3EuB_6O_{12}$ structure contain a three-dimensional framework composed of $[B_5O_{10}]^{5-}$ groups bridged by Eu-O polyhedra (Fig. 2). The $[B_5O_{10}]^{5-}$ group consists of one BO_4 tetrahedron and four BO_3 triangles that form double B-O rings via the common tetrahedron (Fig. 2). Each $[B_5O_{10}]^{5-}$ group is linked to four different Eu-O polyhedra and, likewise, each Eu-O polyhedra is connected to four neighboring $[B_5O_{10}]^{5-}$ groups. The Eu-O polyhedra are formed by the face-sharing linked EuO_6 octahedra. Rubidium cations are located in large cavities of the framework structure (Fig. 2). The main bond lengths obtained for $Rb_3EuB_6O_{12}$ are listed in Table 1S, and one can see a good agreement of refined values with those reported for the structures containing similar $[B_5O_{10}]^{5-}$ units [12].

The unit cell volume dependence on the element combination in $M_3REB_6O_{12}$ (M = alkaline metals; RE = Y, rare earth metals) crystal family is shown in Fig. 3 [33-37,39]. It should be noted that all compounds, besides $K_3TbB_6O_{12}$, have space group *R*32 and similar cell parameters. The K_3(Tb, Lu, Eu)B_6O_{12} compounds have space group $R3_2$ which is non-standard and, moreover, cell parameter *c* is two times smaller in comparison with other compounds [34-36]. The small cell volume of K_3(Tb, Lu, Eu)B_6O_{12} leads to (Tb, Lu, Eu)/K disordering which seems to be not reasonable. As it appears, these structures should be reinvestigated in the future in order to understand the difference. For the analysis shown in Fig. 3, the *c* parameters and unit cell volumes reported for K_3(Tb, Lu, Eu)B_6O_{12} were doubled to uniform the space group *R*32 for $M_3REB_6O_{12}$ crystals. Then, as it is seen from Fig. 3, the cell volume increases with the IR(M) and IR(RE) increase and the curves for Rb and K are practically parallel. In the first approximation, we can write $V = A\times IR(RE) + B\times IR(M) + C$, where A, B, C are some constants. The least-square method was used to estimate A, B, C using the known data about the cell volumes of all known compounds and ions radii of constituted elements [33-37,39]. It was found that general formula $V = 2222.0\times IR(RE) + 1212.6\times IR(M) + 904.7$ Å^3 very well fits the cell volumes of all known compounds, including $Rb_3EuB_6O_{12}$ (Fig. 3). It is interesting that A =

2222.0 is almost two times bigger than B = 1212.6, and this means that the cell volume variation is dominated by changing IR(RE). Moreover, a similar analysis for the cell parameter variation reveals relations a = 1.12617×IR(RE) + 1.51834×IR(M) + 10.10377 Å and c = 9.05935×IR(RE) + 0.91584×IR(M) + 20.86787 Å. The equation for cell parameter c showed that the M cation is of low influence on the c parameter value, but RE provides a ten times bigger effect. In the $M_3REB_6O_{12}$ structure, this effect can be associated with the column of three $(RE)O_6$ octahedra linked by faces, which goes along the c-axis. Probably, increasing RE ion radii cannot be compensated by other ion moving and this leads to a strong c-axis stretching.

Using the diagram shown in Fig. 3, some predictions are possible for the discovery of new NCS borates with the $K_3YB_6O_{12}$ structure. The existence of compounds (RE = Yb, Tm, Er, Ho, Dy, Gd) and $Rb_3REB_6O_{12}$ (RE = Pm, Sm) seems to be evident. Besides, the formation of solid solutions $(K,Rb)_3REB_6O_{12}$ may be reasonably supposed for many RE. The situation with M = Na, Cs is less clear. However, the existence of solid solutions $(Na,Rb)_3REB_6O_{12}$ with averaged IR(Na,Rb) close to that of IR(K) is expected at a high probability. Above this, the existence of solid solutions $(Na,K)_3REB_6O_{12}$ with a partial substitution of Na for K can not be excluded at Na/K ratios when the impact of averaged IR(Na,K) on the structural parameters is not strong.

The synthesized $Rb_3EuB_6O_{12}$ powder possesses light-cream tint, as evident in Fig. 4, that is a common characteristic of Eu-containing oxides [40-42]. A typical SEM image of the particle is shown in Fig. 5. Under the selected technological conditions, the synthesis resulted in the agglomerates of 5-20 μm in size formed by strongly coalescent individual grains with a diameter lower than 1 μm. This micromorphology is common in oxides when the temperature/time conditions used for the solid state reaction are high enough for the active grain interdiffusion [16,34,37,43,44]. It should be pointed that the $Rb_3EuB_6O_{12}$ particles possessed a strong charging effect during SEM measurements and this verifies their very low conductivity common for the oxides without oxygen vacancies.

The recorded DSC curve is shown in Fig. 6. Only a sharp endothermic peak, associated with melting at 1101 K, was observed for $Rb_3EuB_6O_{12}$. The powder XRD pattern measured for the sample obtained by the melt solidification is shown in Fig. 1S. Among the crystalline residues, the presence of $Rb_2(B_4O_5OH)_4)(H_2O)_{3.6}$ (PDF 70-4576), $EuBO_3$ (PDF 74-1931), B_2O_3 (73-1550) was revealed [45-47]. As it is assumed, the $Rb_2(B_4O_5OH)_4)(H_2O)_{3.6}$ compound appeared due to the chemical interaction with the air during cooling because of a high hygroscopicity of the decomposition products. Besides the crystalline compounds, the amorphous component is significant. Thus, it can be concluded that $Rb_3EuB_6O_{12}$ melts incongruently. The thermal parameters, presently available for the $M_3REB_6O_{12}$ borates, are summarized in Table 3. Unfortunately, for $K_3REB_6O_{12}$ compounds, the melting point was earlier measured only for $K_3YB_6O_{12}$. For other $K_3REB_6O_{12}$ borates, however, the melting points can be estimated on the base of the temperature used for solid state synthesis. From the comparison of available experimental data, it can be reasonably assumed that the melting points of $K_3REB_6O_{12}$ borates are noticeably higher than those of $Rb_3REB_6O_{12}$ borates.

The Raman spectrum obtained from $Rb_3EuB_6O_{12}$ is shown in Fig. 7. According to the XRD data, the main structural unit of $Rb_3EuB_6O_{12}$ is the so-called pentaborate group $[B_5O_{10}]^{5-}$ [48], which consists of one BO_4 tetrahedron and four BO_3 triangles (Fig. 2). The ν_1, ν_3, and ν_4 normal vibration modes of planar BO_3 triangles are Raman-active and ν_2, ν_3, and ν_4 are infrared-active; all four normal vibrations of tetrahedral BO_4 groups are Raman-active, whereas only ν_3 and ν_4 are infrared-active [49]. The total set of vibrational modes in $Rb_3EuB_6O_{12}$ is summarized in Table 4. In Fig. 7, for comparison, the Raman frequencies of the pentaborate ion in the potassium pentaborate tetrahydrate single crystal are shown by black vertical lines [50].

The antisymmetric stretching of BO_3 triangles of the pentaborate group is observed in the range of 1300–1700 cm^{-1} in Raman spectra (Fig. 7) and in the range of 1100–1600 cm^{-1} in IR spectra (Fig. 8). These bands intensity are greater in Infrared than in Raman spectra [50]. This region could also be covered by the contribution from the Eu^{3+} $^5D_1 \rightarrow {}^7F_2$ luminescence [41]:

however, the presence of a similar band in the Raman spectrum of $Rb_3NdB_6O_{12}$ indicates its origin both from the boron-oxygen network of the $Rb_3EuB_6O_{12}$ crystal and from the Eu luminescence. The only unexplained lines are narrow doublet at 1290 and 1310 cm^{-1}, that is present in the Raman spectrum of $Rb_3EuB_6O_{12}$, but absent in $Rb_3NdB_6O_{12}$. Strong Raman bands for boron compounds in this region are not known. Therefore, we must ascribe it to the component of the Eu luminescence that experienced a red shift by 100 cm^{-1} in the borate under study, with respect to europium molybdate. However, this suggestion needs an additional study. The Ssymmetric stretching of BO_3 triangles can be found at 875–1000 cm^{-1} in Raman [49, 51] and at 850–975 cm^{-1} in Infrared spectra.

An asymmetric stretching of BO_4 should be observed in Raman spectra in the range of 1000–1150 cm^{-1}. However, these bands intensity are very weak [50]: in the case of Infrared spectra, these vibrations are clearly observed at 975–1100 cm^{-1}. The Raman bands in the region of 725–800 cm^{-1} are the symmetric stretching of BO_4 and a strong line at 756 cm^{-1} can be used as an indicator of the presence of pentaborate group [52]. The symmetric stretching of BO_4, in the range of 750–810 cm^{-1}, can be found in Infrared spectra. The in-plane bending of BO_3 groups locate in the region of 575–650 cm^{-1} in Raman spectra and at 550–625 cm^{-1} in Infrared spectra. The out-of-plane of BO_3 bending should be inactive in Raman and can be found at 650–750 cm^{-1} in Infrared spectra. The Raman bands in the region of 575–650 cm^{-1} in the Raman spectra and spectral region of 550 – 625 cm^{-1} of IR are related to the ν_4 bending modes of BO_4. A strong peak at 530 cm^{-1} is the so-called symmetric pulse vibration of pentaborate anion [53]. The medium bands in the region of 375–500 are ν_2 bending modes of BO_4 groups.

Except for B_5O_{10} vibrations, the Raman spectrum of $Rb_3EuB_6O_{12}$ must contain external vibrations involving the movement of heavy crystal lattice constituents (Eu and Rb). These vibrations are present in the Raman spectrum as the bands observed below 150 cm^{-1}. The Rotational and translational modes of $[B_5O_{10}]^{5-}$ ion as a whole are positioned in the same frequency range, the bending modes are in the range of 200-375 cm^{-1}.

The luminescence spectrum of $Rb_3EuB_6O_{12}$ excited at 514.5 nm is shown in Fig. 9. The infrared part of the spectrum is multiplied by 400 to enhance the visibility of longer-wavelength Eu^{3+} luminescent multiplets. All seven $^5D_0$ - ^7F_J bands are present in this spectrum. A noticeable feature of this spectrum is the prominent ultranarrow line corresponding to the $^5D_0$ - $^7F_0$ transition. The comparison of this line with the same line in the recently studied europium molybdate [41] is presented in Fig. 2S. The ultranarrow line position in the $Rb_3EuB_6O_{12}$ borate is at 579.8 nm and its width is 5 cm^{-1} (FWHM), while, in α-$Eu_2(MoO_4)_3$, it is at 580.4 nm with the width of 2 cm^{-1}. As one can extract from the structural results, Eu ions occupy three inequivalent sites within the unit cell of the $Rb_3EuB_6O_{12}$ crystal. Two of them are featured by the C_3 local symmetry of Eu^{3+} ion, while the third one possesses the D_3 local symmetry. The selection rules allow the $^5D_0$ - $^7F_0$ transition only in case of the symmetry as low as C_3, but not in the case of D_3. Therefore, the observed ultranarrow line must be ascribed to the first two sites with the required symmetry.

In most crystals and glasses containing Eu^{3+} ions, the hypersensitive $^5D_0$ - $^7F_2$ transition is typically the most intense since its oscillator strength is due to the lack of inversion symmetry, and such Eu^{3+} ion environment is rather common. This is the case of our borate, too. However, comparing the spectra of $Rb_3EuB_6O_{12}$ and earlier studied α-$Eu_2(MoO_4)_3$, we see that the ultranarrow line intensity, with respect to hypersensitive band, is much higher in borate than that in molybdate. To reveal the nature of this feature, we recorded the luminescence spectra of equal amounts of both materials at the same spectrometer settings in order to enable an approximate comparison of the lines intensities (difference in the Eu content and in the absorption cross sections was not accounted for). The hypersensitive band intensity is 43.7 times smaller in borate than in molybdate, while the ultranarrow line intensity is only 2.1 times smaller. Since both emissions originate from the same starting level, we can deduce that breaking the central inversion of the local environment of all three inequivalent Eu sites in $Rb_3EuB_6O_{12}$ leads to a smaller oscillator strength gain of the hypersensitive transition than the mirror symmetry

breaking in C_3 sites, with respect to the same symmetry violations in a single C_1 site of Eu in α-$Eu_2(MoO_4)_3$.

Another interesting feature of borate $Rb_3EuB_6O_{12}$ is the shape of hypersensitive $^5D_0$ - $^7F_2$ transition band which is dominated by a single narrow peak at 611 nm, as shown in Fig. 9, This feature is, in principle, favorable for obtaining the lasing at this transition since the amplification cross section is not smeared over a wide spectral region, but it is concentrated in the peaking wavelength vicinity (Fig. 3S). However, due to the above-described fact that the concentration quenching in $Rb_3EuB_6O_1$ is stronger than in α-$Eu_2(MoO_4)_3$, the use of a lower Eu content must be recommended, e.g. by diluting Eu^{3+} with Gd^{3+} which possesses the closest ionic radius.

4. Conclusions

In the $K_3YB_6O_{12}$ borate family, new noncentrosymmetric Rb-containing borates $Rb_3REB_6O_{12}$ (RE = Nd, Eu) were discovered and this greatly extends the nomenclature of the noncentrosymmetric borate crystals available in this family. As it is clear, this borate family covers a wide range of RE elements, including those appropriate for laser and photonic applications. Thus, a more wide and deep investigation of the compounds related to the $M_3REB_6O_{12}$ (M = alkaline metals; RE = Y, rare earth metals) crystal family is topical, including a search for new compounds and solid solutions, development of the crystal growth methods, the observation of piezoelectric and luminescence characteristics. This opens a door for the estimation of this borate family potential for practical applications. The luminescence properties of Eu ion, along with nonlinear properties of the matrix, indicate that Eu-activated crystals of the $Rb_3REB_6O_{12}$ family (RE = Gd, La and probably Y and Lu) are good candidates for self-doubling Eu-lasing media.

Acknowledgements

We are grateful to Guochun Zhang for the crystal structure materials on $K_3YB_6O_{12}$ and O. Tsydenova, A. Sarapulova for the consultations. The work was supported by Project № 0356-2015-0412 of SB RAS Program № II.2P. The reported study was funded by RFBR according to research projects 16-52-48010, 17-02-00920 and 17-52-53031.

References

1. C. Chen, Z. Lin, Z. Wang, The development of new borate-based UV nonlinear optical crystals, Appl. Phys. B 80 (2005) 1–25.
2. Wenjiao Yao, Ran He, Xiaoyang Wang, Zheshuai Lin, Chuangtian Chen, Analysis of deep-UV nonlinear optical borates: approaching the end, Adv. Opt. Mater. 2 (5) (2014) 411-417.
3. Zheshuai Lin, Jiao Lin, Zhizhong Wang, Chuangtian Chen, Ming-Hsien Lee, Mechanism for linear and nonlinear optical effects if LiB_3O_5, CsB_3O_5, and $CsLiB_6O_{10}$ crystals, Phys. Rev. B 62 (3) (2000) 1757-1764.
4. Z.S. Lin, Z.Z. Wang, C.T. Chen, M.H. Lee, Mechanism for linear and nonlinear optical effects in monoclinic bismuth borate (BiB_3O_6) crystal, J. Appl. Phys. 90 (11) (2001) 5585-5590.
5. V.V. Atuchin, L.D. Pokrovsky, V.G. Kesler, N.Yu. Maklakova, M. Yoshimura, N. Ushiyama, T. Matsui, K. Kamimura, Y. Mori, T. Sasaki, Cesium accumulation at CsB_3O_5 optical surface, Opt. Mater. 23 (2003) 377-383.
6. V.V. Atuchin, L.D. Pokrovsky, V.G. Kesler, L.I. Isaenko, L.I. Gubenko, Structure and chemistry of LiB_3O_5 (LBO) optical surfaces, J. Ceram. Proc. Research 4 (2003) 84-87.
7. V.V. Atuchin, V.G. Kesler, A.E. Kokh, L.D. Pokrovsky, X-ray photoelectron spectroscopy study of β-BaB_2O_4 optical surface, Appl. Surf. Sci. 223 (2004) 352-360.
8. P. A. Popov, N. V. Moiseev, A. E. Kokh, K. A. Kokh, Thermal conductivity and heat capacity of α- and β-BaB_2O_4 cingle crystals, Inorg. Mater. 47 (2) (2011) 163-166.
9. Xin Zhang, Lirong Wang, Shufeng Zhang, Guiling Wang, Sangen Zhao, Yong Zhu, Yicheng Wu, Chuangtian Chen, Optical properties of the vacuum-ultraviolet nonlinear optical crystal - BPO_4, J. Opt. Soc. Am. B 28 (9) (2011) 2236-2239.
10. A.S. Aleksandrovsky, A.M. Vyunishev, A.I. Zaitsev, Applications of random nonlinear photonic crystals based on strontium tetraborate, Crystals 2 (4) (2012) 1393-1409.

11. A.I. Zaitsev, A.S. Aleksandrovsky, A.S. Kozhukhov, L.D. Pokrovsky, V.V. Atuchin, Growth, optical and microstructural properties of PbB_4O_7 plate crystals, Opt. Mater. 37 (2014) 298-301.
12. J.D. Grice, P.C. Burns, F.C. Hawthorne, Borate minerals. II. A hierarchy of structures based upon the borate fundamental building block 37 (3) (1999) 731-762.
13. P. Becker, A contribution to borate crystal chemistry: Rules for the occurrence of polyborate anion types, Z. Kristallogr. 216 (2001) 523-533.
14. V.V. Atuchin, B.I. Kidyarov, N.V. Pervukhina, Phenomenological modeling and design of new acentric crystals for optoelectronics, Comput. Mater. Sci. 30 (2004) 411-418.
15. A.S, Korotkov, V.V. Atuchin, Distribution and structures of acentric borates for non-linear laser optics, Proc. SPIE 6258 (2006) 62580B.
16. V.V. Atuchin, B.G. Bazarov, T.A. Gavrilova, V.G. Grossman, M.S. Molokeev, Zh.G. Bazarova, Preparation and structural properties of nonlinear optical borates $K_{2(1-x)}Rb_{2x}Al_2B_2O_7$, $0 < x < 0.75$, J. Alloys Compd. 515 (25) (2012) 119–122.
17. R.V. Kurbatov, L.A. Solovyov, B.G. Bazarov, A.K. Subanakov, J.G. Bazarova, Synthesis, structure and properties of $RbMgBO_3$, Solid State Comm. 172 (2013) 33–36.
18. A.V. Malakhovskii, T.V. Kutsak, A.L. Sukhachev, A.S. Aleksandrovsky, A.S. Krylov, I.A. Gudim, M.S. Molokeev, Spectroscopic properties of $ErAl_3(BO_3)_4$, Chem. Phys. 428 (2014) 137-143.
19. D.A. Ikonnikov, A.V. Malakhovskii, A.L. Sukhachev, V.L. Temerov, A.S. Krylov, A.F. Bovina, A.S. Aleksandrovsky, Spectroscopic properties of $HoAl_3(BO_3)_4$, Opt. Mater. 37 (2014) 257-261.
20. Hongwei Yu, Hongping Wu, Shilie Pan, Zhihua Yang, Xueling Hou, Xin Su, Qun Jing, Kenneth R. Poeppelmeier, James M. Rondinelli, $Cs_3Zn_6B_9O_{21}$: A chemically benign of KBBF family exhibiting the largest second harmonic generation response, J. Am. Chem. Soc. 136 (4) (2014) 1264-1267.

21. Sangen Zhao, Pifu Gong, Lei Bai, Xiang Xu, Shuquan Zhang, Zhihua Sun, Zheshuai Lin, Maochun Hong, Chuangtian Chen, Junhua Luo, Berullium-free $Li_4Sr(BO_3)_2$ for deep-ultraviolet nonlinear optical applications, Nature Commun. 5 (2014) 4019.
22. Hongwei Yu, Weiguo Zhang, Joshua Young, James M. Rondinelli, P. Shiv Halasyamani, Design and synthesis of the beryllium-free deep-ultraviolet nonlinear optical material $Ba_3(ZnB_5O_{10})PO_4$, Adv. Mater. 27 (45) (2015) 7380-7385.
23. T. Thao Tran, Nathan Z. Koocher, James M. Rondinelli, P. Shiv Halasyamani, Beryllium-free β-$Rb_2Al_2B_2O_7$ as a possible deep-violet nonlinear optical material replacement for $KBe_2BO_3F_2$, Angew. Chem. Int. Ed. 129 (11) (2017) 3015-3019.
24. A.D. Mills, Crystallographic data for new rare earth borate compounds, $RX_3(BO_3)_4$, Inorg. Chem. 1 (1962) 960–961.
25. R. Norrestam, M. Nygren, J.O. Bovin, Structural investigations of new calcium-rare earth (R) oxyborates with the composition $Ca_4RO(BO_3)_3$, Chem. Mater. 4 (1992) 737-743.
26. P. Gravereau, J.-P. Chaminade, S. Pechev, V. Nikolov, P. Peshev, $Na_3La_9O_3(BO_3)_8$, a new oxyborate in the ternary system Na_2O-La_2O_3-B_2O_3: preparation and crystal structure, Solid State Sci. 4 (2002) 993–998.
27. A.S. Aleksandrovsky, I.A. Gudim, A.S. Krylov, V.L. Temerov, Luminescence of yttrium aluminum borate syngle crystals doped with manganese, Phys. Solid State 49 (9) (2007) 1695-1699.
28. A.S. Aleksandrovsky, I.A. Gudim, A.S. Krylov, A.V. Malakhovskii, V.L. Temerov, Upconversion luminescence of $YAl_3(BO_3)_4$:(Yb^{3+},Tm^{3+}) crystals, J. Alloys Compd. 496 (2010) 118-121.
29. Zhongben Pan, Jie Ma, Honghao Xu, Dingyuan Tang, Huaqiang Cai, Haohai Yu, Huaijin Zhang, Jiyang Wang, 251 fs pulse generation with a Nd^{3+}-doped $Ca_3Gd_2(BO_3)_4$ disordered crystal, RSC Adv. 5 (2015) 44137-44141.

30. Zhihua Li, Jinghui Zeng, Guochun Zhang, Yadong Li, A new promising phosphor, $Na_3La_2(BO_3)_3$:*Ln* (Ln = Eu, Tb), J. Solid State Chem. 178 (2005) 3624–3630.
31. J.H. Gao, R.K. Li, $Rb_3Y_2(BO_3)_3$ with a noncentrosymmetric structure, Acta Crystallogr. C 63 (2007) i112–i114.
32. Jianxiu Zhang, Guiling Wang, Zuoliang Liu, Lirong Wang, Guochun Zhang, Xin Zhang, Yang Wu, Peizhen Fu, Yicheng Wu, Growth and optical properties of a new nonlinear $Na_3La_9O_3(BO_3)_8$ crystal. Opt. Express 18 (1) (2010) 237–243.
33. S.G. Zhao, G.C. Zhang, J.Y. Yao, Y.C. Wu, $K_3YB_6O_{12}$: A new nonlinear optical crystal with a short UV cutoff edge, Mat. Res. Bull. 47 (11) (2012) 3810–3813.
34. Dan Zhao, Fa-Xue Ma, Zhi-Qiang Wu, Lei Zhang, Wei Wei, Juan Yang, Rong-Hua Zhang, Peng-Fei Chen, Shan-Xuan Wu, Synthesis, crystal structure and characterizations of new red phosphor $K_3EuB_6O_{12}$, Mater. Chem. Phys. 182 (2016) 231-236.
35. Dan Zhao, Fa-Xue Ma, Rui-Juan Zhang, Min Huang, Peng-Fei Chen, Rong-Hua Zhang, Wei Wei, Substitution disorder and photoluminescent property of a new rare-earth borate: $K_3TbB_6O_{12}$, Z. Kristallogr. 231 (9) (2016) 525-530.
36. Dan Zhao, Fa-Zue Ma, Rui-Juan Zhang, Wei Wei, Juan Yang, Ying-Jie Li, A new rare-earth borate $K_3LuB_6O_{12}$: crystal and electronic structure, and luminescent properties activated by Eu^{3+}, J. Mater. Sci.: Mater. Electron. 28 (1) (2017) 129-136.
37. V.V. Atuchin, A.K. Subanakov, A.S. Aleksandrovsky, B.G. Bazarov, J.G. Bazarova, S.G. Dorzhieva, T.A. Gavrilova, A.S. Krylov, M.S. Molokeev, A.S. Oreshonkov, A.M. Pugachev, Yu.I. Tushinova, A.P. Yelisseyev, Exploration of structural, thermal, vibrational and spectroscopic properties of new noncentrosymmetric double borate $Rb_3NdB_6O_{12}$, Adv. Powder Technol. 28 (2017) 1309-1315.
38. Bruker AXS TOPAS V4: General profile and structure analysis software for powder diffraction data. – User's Manual. Bruker AXS, Karlsruhe, Germany. 2008.

39. R.D. Shannon, Revised effective ionic radii and systematic studies of interatomic distancies in halides and chalcogenides, Acta Cryst. A 32 (1976) 751-767.
40. T.N. Khamaganova, N.M. Khrushcheva, Z.G. Bazarova, Mixed borates of composition $Sr_3R(BO_3)_3$ (R = Pr-Lu, Y, Sc), Russ. J. Inorg. Chem. 44 (10) (1999) 1542-1543.
41. V.V. Atuchin, A.S. Aleksandrovsky, O.D. Chimitova, T.A. Gavrilova, A.S. Krylov, M.S. Molokeev, A.S. Oreshonkov, B.G. Bazarov, J.G. Bazarova, Synthesis and spectroscopic properties of monoclinic α-$Eu_2(MoO_4)_3$, J. Phys. Chem. C 118 (2014) 15404-15411.
42. Haipeng Ji, Zhaohui Huang, Zhiguo Xia, Maxim S. Molokeev, Xingxing Jiang, Zheshuai Lin, Victor V. Atuchin, Comparative investigations of the crystal structure and photoluminescence property of eulytite-type $Ba_3Eu(PO_4)_3$ and $Sr_3Eu(PO_4)_3$, Dalton Trans. 44 (16) (2015) 7679-7686.
43. V.V. Atuchin, V.G. Grossman, S.V. Adichtchev, N.V. Surovtsev, T.A. Gavrilova, B.G. Bazarov, Structural and vibrational properties of microcrystalline $TlM(MoO_4)_2$ (M = Nd, Pr) molybdates, Opt. Mater. 34 (5) (2012) 812-816.
44. E.N. Galashov, V.V. Atuchin, T.A. Gavrilova, I.V. Korolkov, Y.M. Mandrik, A.P. Yelisseyev, Zhiguo Xia, Synthesis of $Y_3Al_5O_{12}:Ce^{3+}$ phosphor in the Y_2O_3-Al metal-CeO_2 ternary system, J. Mater. Sci. (2017) DOI: 10.1007/s10853-017-1427-5.
45. M. Touboul, N. Penin, G. Nowogrocki, Crystal structure and thermal behavior of $Rb_2[B_4O_5(OH)_4]\cdot 3.6H_2O$, J. Solid State Chem. 149 (1) (2000) 197-202.
46. R.E. Newnham, M.J. Redman, R.P. Santoro, Crystal structure of yttrium and other rare-earth borates. J. Am. Ceram. Soc. 46 (6) (1963) 253-256.
47. S.V. Berger, The crystal structure of boron oxide, Acta Chem. Scand. *7* (1953) 611-622.
48. B.N. Meera, A.K. Sood, N. Chandrabhas, J. Ramakrishna, Raman study of lead borate glasses, J Non-Cryst. Solids 126 (1990) 224-230.
49. K. Nakamoto, Infrared and Raman Spectra of Inorganic and Coordination Compounds, 6th edn. Wiley, New York etc., 2009.

50. V. Devarajan, E. Gräfe, E. Funck, Raman spectrum and normal coordinate analysis of pentaborate ion (B_5O_{10}) in potassium pentaboratetetrahydrate, Spectrochim. Acta A 32 (1976) 1225-1233.
51. K.B. Petrosyan, K.M. Pokhsraryan, Stimulated Raman scattering in a potassium pentaborate crystal, Phys. Stat. Sol. (b) 127 (1985) K105–K108.
52. R. Thomas, P. Davidson and A.Hahn, Ramanite-(Cs) and ramanite-(Rb): New cesium and rubidium pentaborate tetrahydrate minerals identified with Raman spectroscopy, Am. Mineral 93 (2008) 1034–1042.
53. Li Jun, Xia Shuping and Gao Shiyang, FT-IR and Raman spectroscopic study of hydrated borates, Spectrochim. Acta A 51 (1995) 519-532.

Table 1. Crystallographic data obtained for $Rb_3EuB_6O_{12}$ phase at room temperature

Compound	$Rb_3EuB_6O_{12}$
Sp. Gr.	*R*32
a, Å	13.4732 (2)
c, Å	30.8424 (6)
V, Å^3	4848.6 (2)
Z	3
2θ-interval, º	5-100
No. of reflections	658
No. of refined parameters	98
R_{wp}, %	2.26
R_p, %	1.63
R_{exp}, %	0.62
χ^2	3.66
R_B, %	1.07

Table 2. Fractional atomic coordinates and isotropic displacement parameters (Å^2) of $Rb_3EuB_6O_{12}$

	x	*y*	*z*	B_{iso}
		$Rb_3EuB_6O_{12}$		
Eu1	1/3	2/3	-0.2182 (7)	0.5 (5)
Eu2	1/3	2/3	-0.7192 (7)	0.5 (5)
Eu3	1/3	2/3	2/3	1.5 (8)
Rb1	0.116 (1)	1/3	5/6	1.5 (7)
Rb2	2/3	0.798 (2)	1/3	1.5 (6)
Rb3	0.187 (1)	0.855 (1)	-0.4146 (6)	1.5 (3)
Rb4	1/3	2/3	-0.580 (1)	1.5 (4)
Rb5	1/3	2/3	1/6	0.9 (11)
B1	0.19 (2)	0.78 (2)	-0.278 (5)	2.0 (9)
B2	0.21 (2)	0.77 (2)	-0.514 (6)	2.0 (9)
B3	0.47 (2)	0.89 (2)	-0.651 (6)	2.0 (9)
B4	0.66 (2)	1.08 (1)	-0.419 (6)	2.0 (9)
B5	0.47 (2)	0.93 (1)	-0.891 (5)	2.0 (9)
O1	0.27 (1)	0.769 (8)	-0.482 (2)	1.5 (5)
O2	0.170 (7)	0.566 (8)	-0.682 (2)	1.5 (5)
O3	0.391 (7)	0.806 (4)	-0.388 (2)	1.5 (5)
O4	0.284 (6)	0.773 (5)	-0.769 (2)	1.5 (5)
O5	0.516 (7)	0.855 (7)	-0.620 (3)	1.5 (5)
O6	0.521 (7)	0.851 (8)	-0.542 (3)	1.5 (5)
O7	0.497 (6)	1.010 (5)	-0.648 (2)	1.5 (5)
O8	0.667 (6)	0.808 (5)	-0.525 (2)	1.5 (5)
O9	0.592 (6)	1.036 (9)	-0.579 (3)	1.5 (5)
O10	0.099 (8)	0.730 (6)	-0.750 (3)	1.5 (5)

Table 3. Thermal parameters obtained for borates with general composition $MREB_6O_{12}$ (M = K, Rb RE = Y, rare earths)

$M_3REB_6O_{12}$	Melting temperature, K	Enthalpy, J/g	Reference
$K_3EuB_6O_{12}$	>1023	-	[34]
$K_3TbB_6O_{12}$	>1023	-	[35]
$K_3YB_6O_{12}$	1214	-	[33]
$K_3LuB_6O_{12}$	>1023	-	[36]
$Rb_3NdB_6O_{12}$	1070	–122.4	[37]
$Rb_3EuB_6O_{12}$	1101	–160.6	This work

Table4. Wyckoff positions of atoms and vibrational modes in $Rb_3EuB_6O_{12}$

Atom	Wyckoff position	Mechanical representation
Rb1	9e	$A_1 + 2A_2 + 3E$
Rb2	9d	$A_1 + 2A_2 + 3E$
Eu1, Eu2, Rb4	6c	$A_1 + A_2 + 2E$
Rb5	3b	$A_2 + E$
Eu3	3a	$A_2 + E$
Rb3, B1–B5, O1–O10	18f	$3A_1 + 3A_2 + 6E$
Total		$53A_1 + 57A_2 + 110E$
Acoustic		$A_2 + E$
Optic		$53A_1 + 56A_2 + 109E$
Raman active modes		$53A_1 + 109E$
IR active modes		$56A_2 + 109E$

Captions

Fig. 1. Measured (red), calculated (black) and differential (blue) diffraction patterns of $Rb_3EuB_6O_{12}$.

Fig. 2. $Rb_3EuB_6O_{12}$ crystal structure.

Fig. 3. The dependence of unit cell volume V on the element combination in $M_3REB_6O_{12}$ (M = alkaline metals; RE = Y, rare earth metals) crystal family.

Fig. 4. The digital image of $Rb_3EuB_6O_{12}$ powder under illumination by white light.

Fig. 5. SEM pattern of the $Rb_3EuB_6O_{12}$ particle.

Fig. 6. DSC measurements in the temperature range of 298 – 813 K.

Fig. 7. $Rb_3EuB_6O_{12}$ Raman spectra in comparison with the band positions of pentaborate ion in the potassium pentaborate tetrahydrate single crystal [50].

Fig. 8. $Rb_3REB_6O_{12}$ (RE = Nd, Eu) IR spectra.

Fig. 9. High-resolution PL spectrum for $Rb_3EuB_6O_{12}$ recorded at excitation 514.5 nm with a T64000 spectrometer. The long-wavelength part is multiplied by 400 and shifted up.

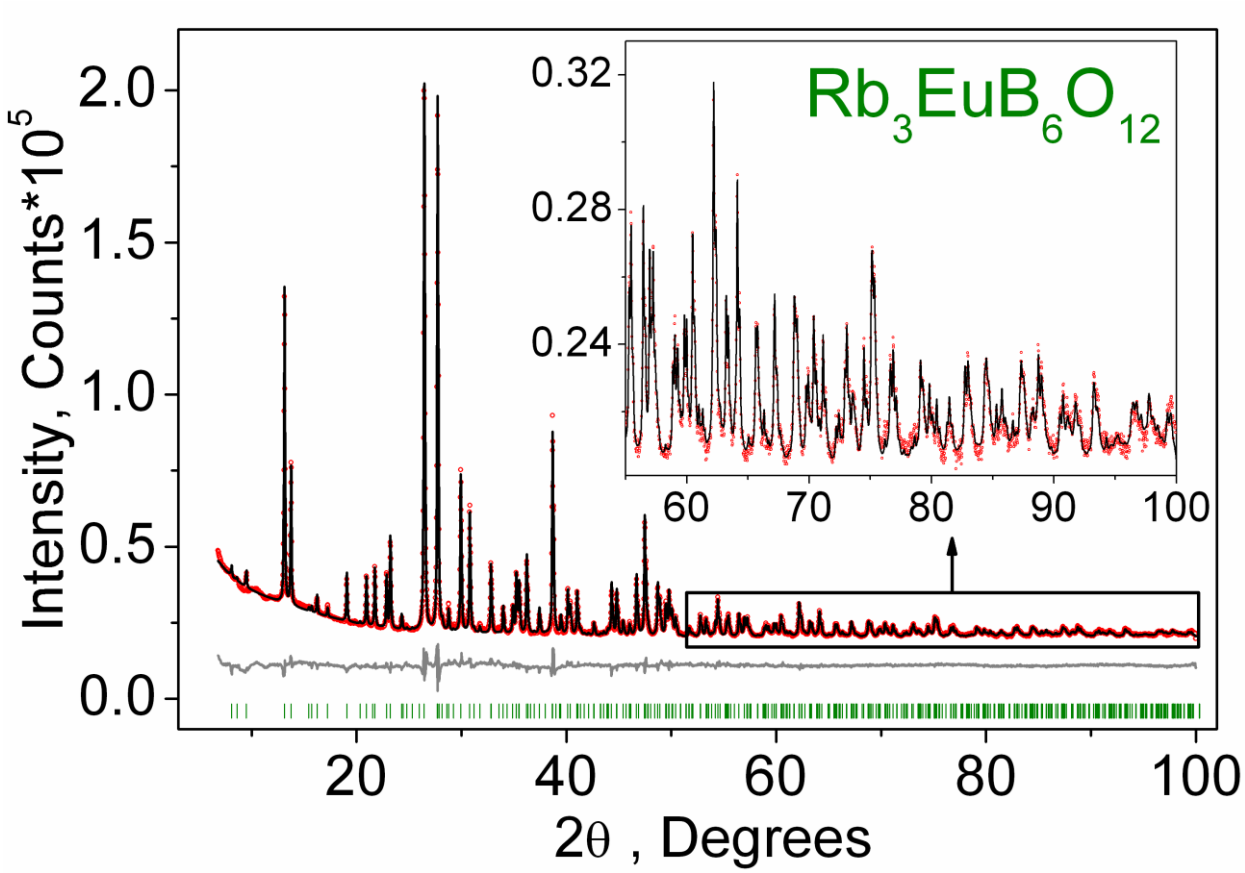
Rb3EuB6O12
Intensity, Counts*10^5
2θ , Degrees
0.0
0.5
1.0
1.5
2.0
20
40
60
80
100
0.24
0.28
0.32
60
70
80
90
100

Fig. 1.

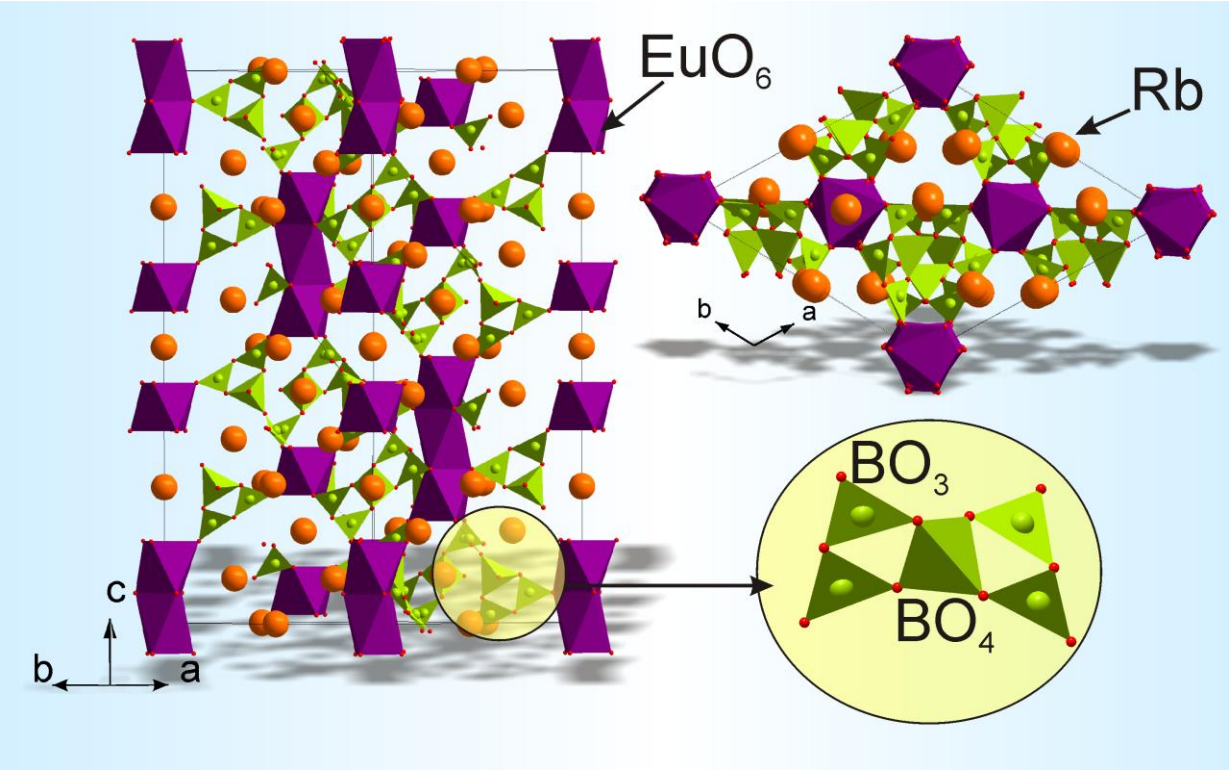

Fig. 2.

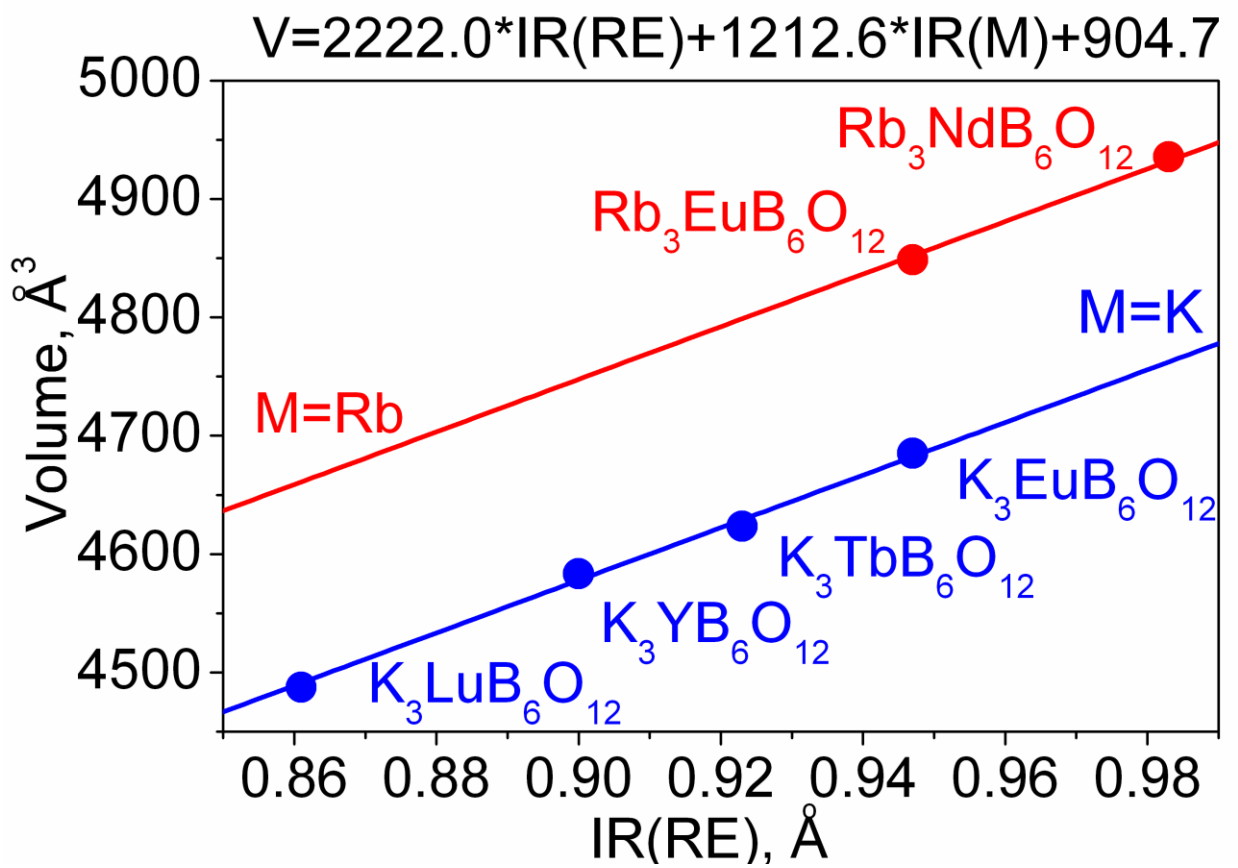
V=2222.0*IR(RE)+1212.6*IR(M)+904.7
Volume, Å3
5000
4900
4800
4700
4600
4500
0.86
0.88
0.90
0.92
0.94
0.96
0.98
IR(RE), Å
Rb3NdB6O12
Rb3EuB6O12
M=K
M=Rb
K3EuB6O12
K3TbB6O12
K3YB6O12
K3LuB6O12

Fig. 3.

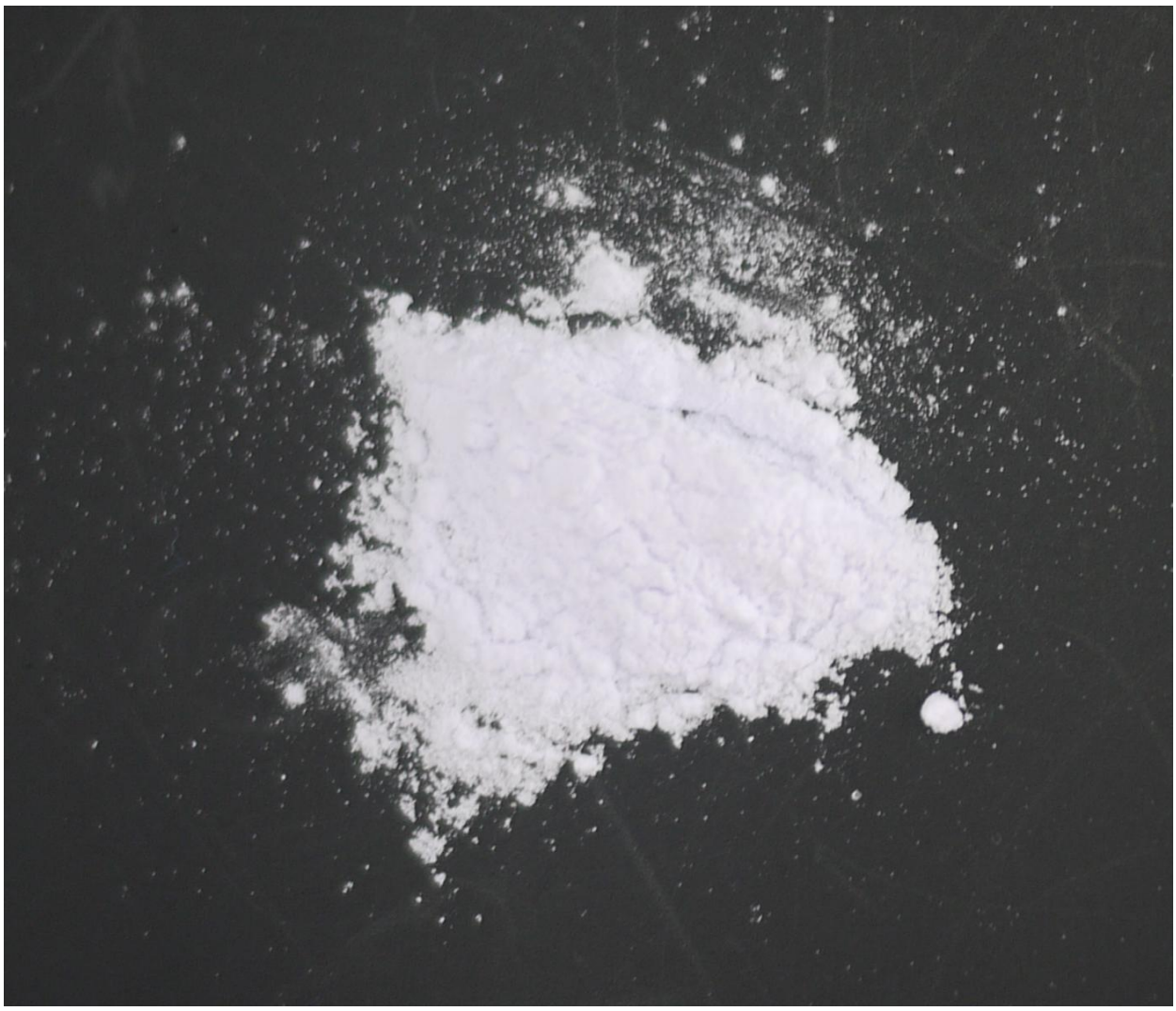

Fig. 4.

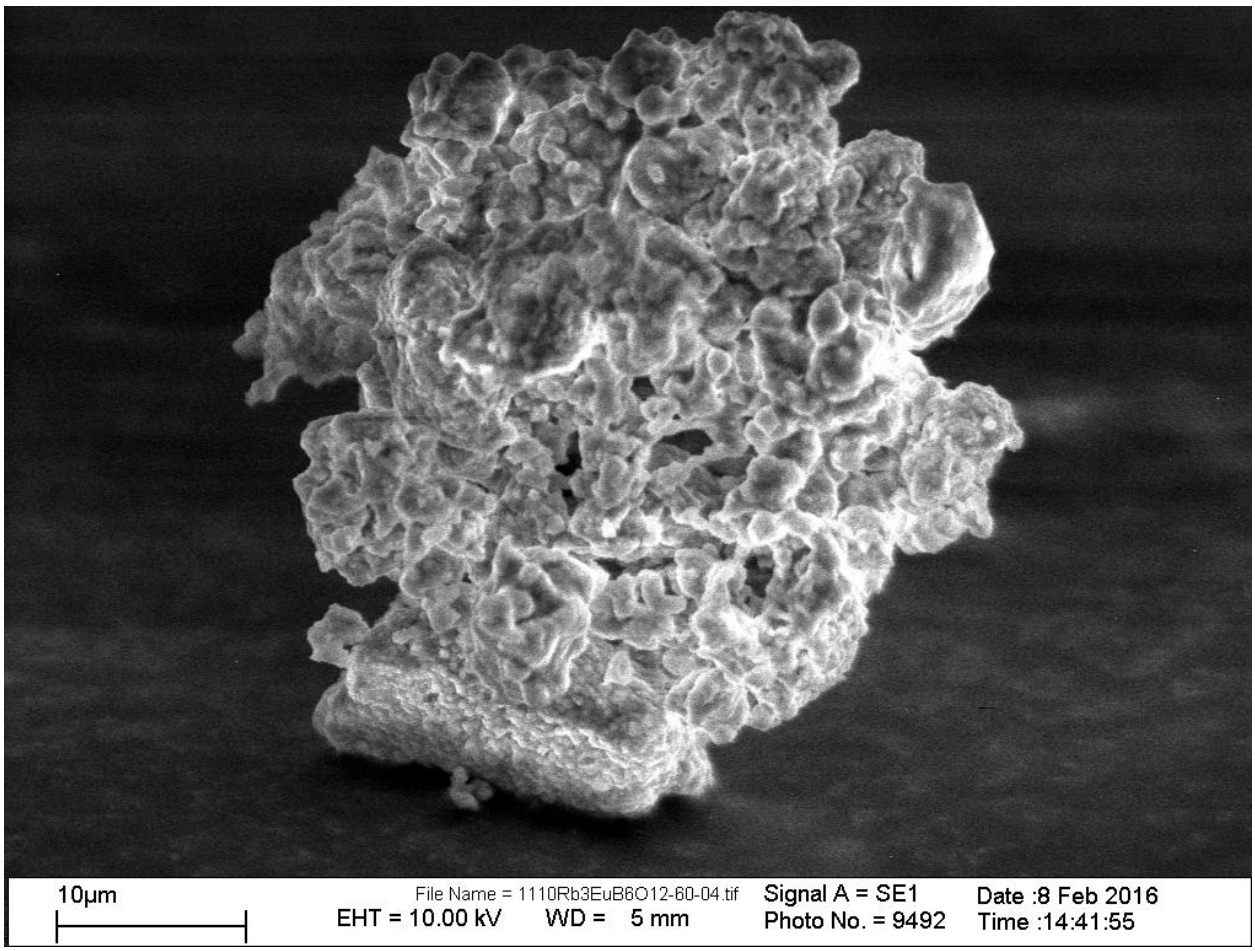
10µm
File Name = 1110Rb3EuB6O12-60-04.tif
EHT = 10.00 kV
WD = 5 mm
Signal A = SE1
Photo No. = 9492
Date :8 Feb 2016
Time :14:41:55

Fig. 5.

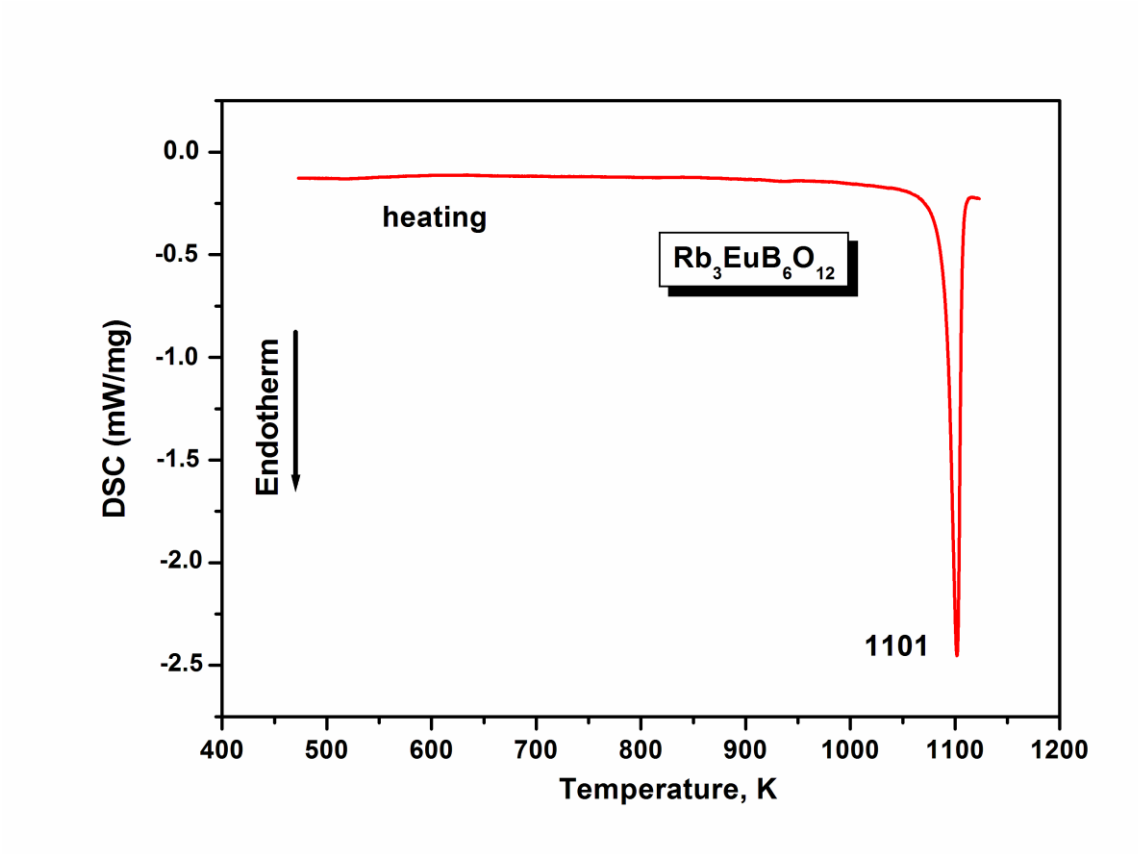
0.0
-0.5
-1.0
-1.5
-2.0
-2.5
DSC (mW/mg)
heating
Rb3EuB6O12
Endotherm
1101
400
500
600
700
800
900
1000
1100
1200
Temperature, K

Fig. 6.

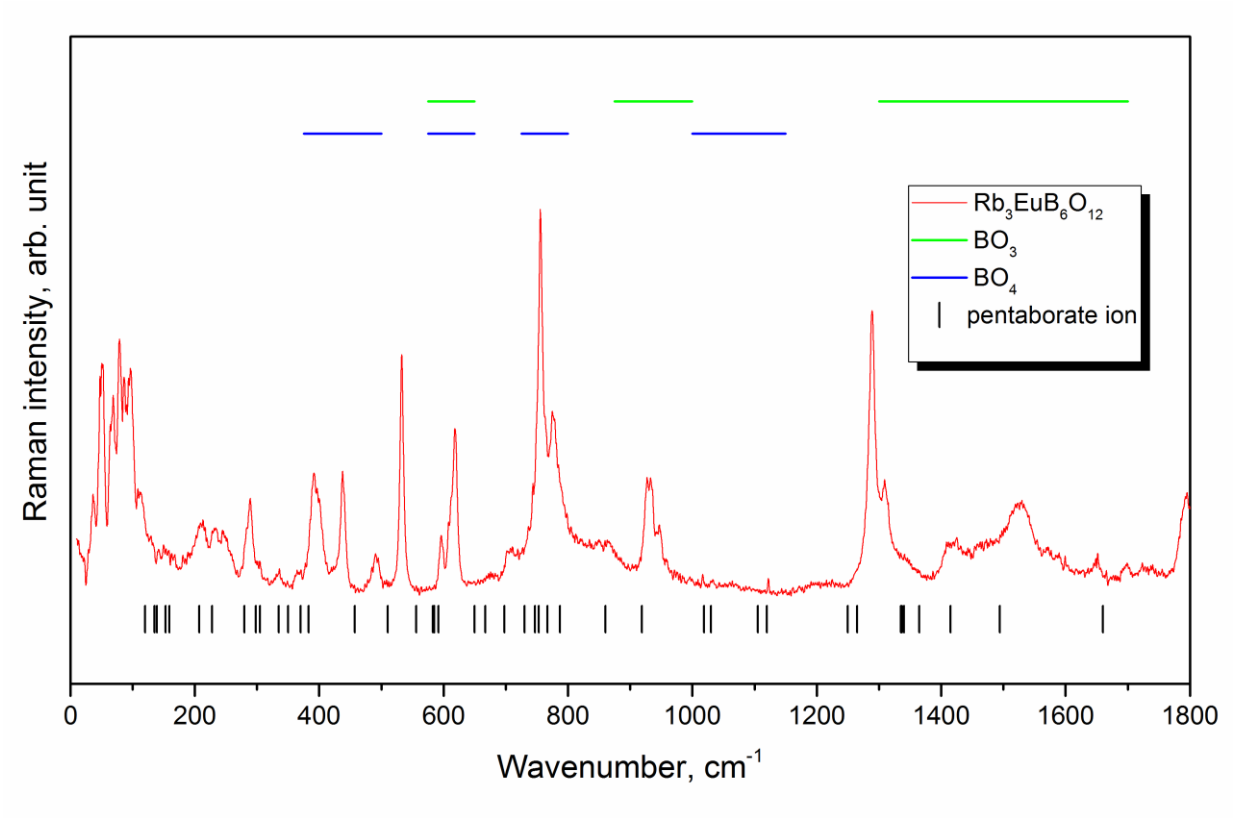
Raman intensity, arb. unit
Wavenumber, cm-1
0
200
400
600
800
1000
1200
1400
1600
1800
Rb3EuB6O12
BO3
BO4
pentaborate ion

Fig. 7.

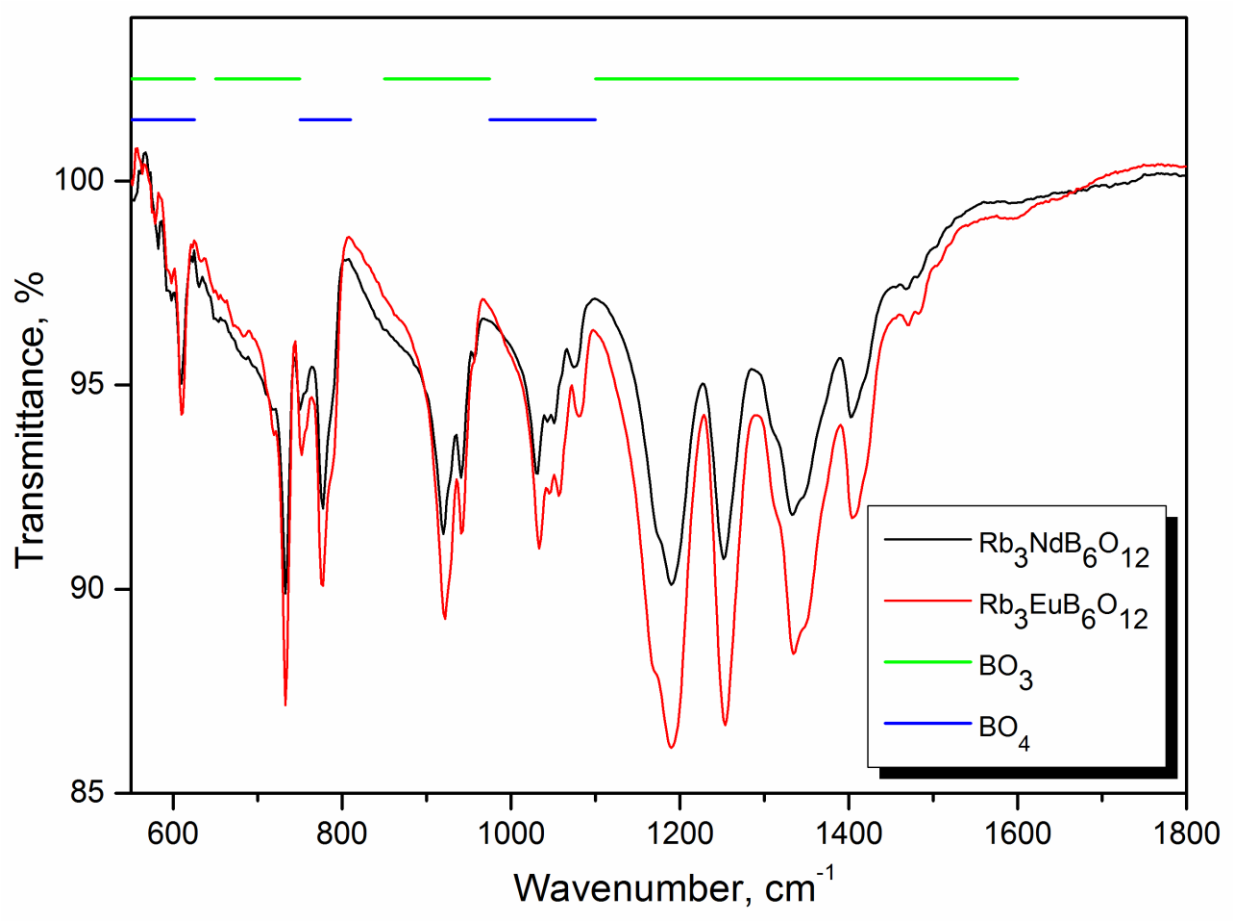
Transmittance, %
100
95
90
85
600
800
1000
1200
1400
1600
1800
Wavenumber, cm-1
Rb3NdB6O12
Rb3EuB6O12
BO3
BO4

Fig. 8.

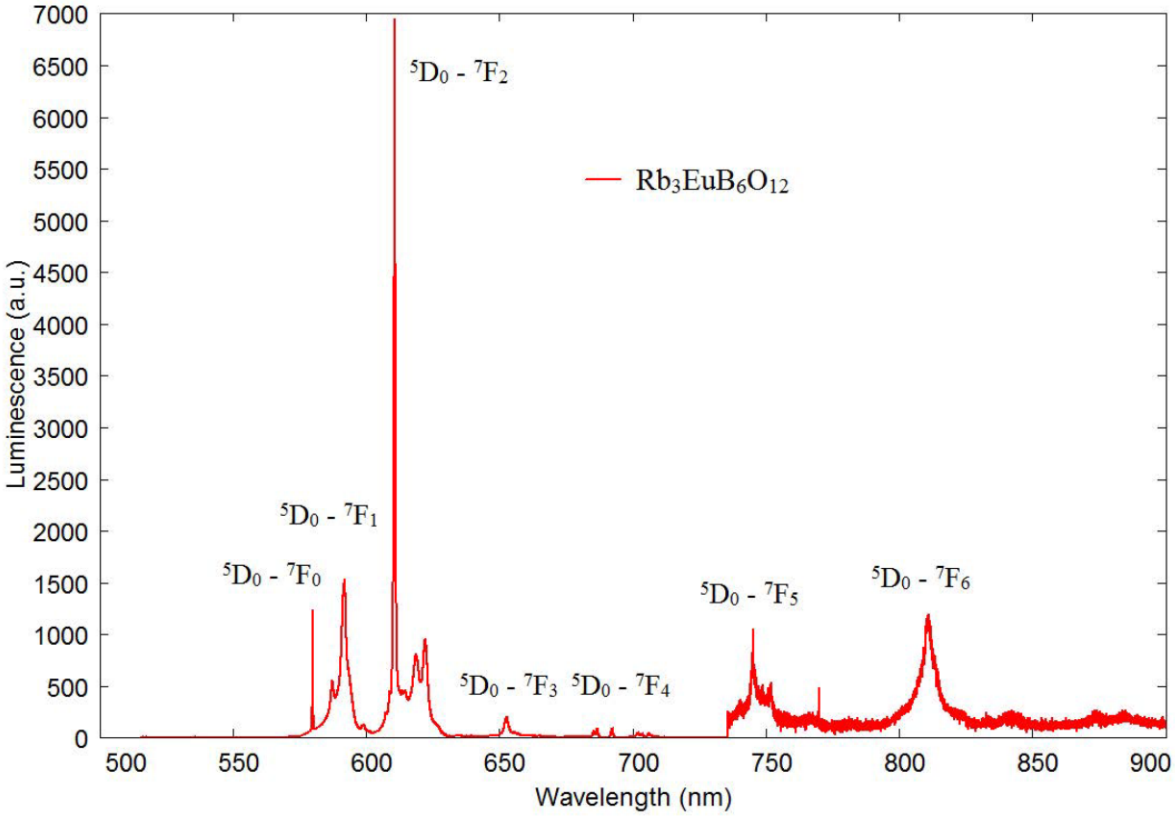
Luminescence (a.u.)
Wavelength (nm)
$^5D_0$ - $^7F_2$
$Rb_3EuB_6O_{12}$
$^5D_0$ - $^7F_1$
$^5D_0$ - $^7F_0$
$^5D_0$ - $^7F_5$
$^5D_0$ - $^7F_6$
$^5D_0$ - $^7F_3$
$^5D_0$ - $^7F_4$

Fig. 9.